Preliminary study of a visible, high spatial resolution spectrometer for DEMO divertor survey

W. Gonzalez,[a,1] **W. Biel,**[a] **Ph. Mertens,**[a] **M. Tokar,**[a] **O. Marchuk,**[a] **F. Mourão**[b] **and Ch. Linsmeier**[a]

[a]*Forschungszentrum Jülich GmbH, Institut für Energie- und Klimaforschung — Plasmaphysik,*
52425 Jülich, Germany

[b]*Instituto de Plasmas e Fusão Nuclear (IPFN), Instituto Superior Técnico, Universidade de Lisboa*
1049-001 Lisboa, Portugal

E-mail: winder.gonzalez@gmail.com

ABSTRACT: Developments towards DEMO Diagnostic and Control (D&C) system conceptual design are based on a subset of ITER mature diagnostic systems, whose eligibility for DEMO has been endorsed by their robustness, long lifetime expectancy and feasible remote maintenance [1]. They are devoted to ensure the machine operation in compliance with safety requirements and high availability. In particular, the evolution of divertor spectroscopic measurements on fusion experiments has demonstrated their potential as a control method for divertor protection via detachment control [2, 3] (near ultraviolet, 300–400 nm) and monitoring of the plasma-wall interaction (visible range, 400–700 nm) [4]. These characteristics make this method one of the leading candidates for DEMO detachment and radiation control power. In line with the application of a system engineering approach [5], initial assessments of design and feasibility of a VIS high spatial resolution spectrometer for the DEMO divertor survey based on early DEMO control requirements are presented and discussed. The proposed system is located at the equatorial port and it is composed of 3 oblique lines of sights (LoS), 9 toroidal mirrors, 6 plane mirrors and 6 spectrometers examining the outer, inner and X-point divertor region, optimized for the monitoring of chord-integrated NUV/VIS signals under parallel divertor plasmas observation. The wavelengths of interest, spatial resolution and main integration issues are reported.

KEYWORDS: Plasma diagnostics - interferometry, spectroscopy and imaging; Plasma diagnostics - charged-particle spectroscopy

---

[1]Corresponding author.

Contents

1 Introduction

The demonstration fusion reactor (DEMO) in comparison to ITER will have to prove high robustness and reliability operation near technical and physics limits, over a significant pulse duration [6], with a reduced number of diagnostic systems exclusively for safety and plasma control [7]. In this context, the progress of DEMO design and R&D activities are aimed to provide an early DEMO diagnostic and control (D&C) concept supported by a system engineering approach, based on mature technologies and reliable regimes of operation extrapolated from the future ITER experience [5].

In this phase of DEMO D&C development a prime choice of diagnostic methods applicable to the stationary burn phase of the discharge has been obtained [1]. This preliminary group of D&C systems comprises a large range of diagnostic techniques, the control function of which and integration approaches are in constant evolution. In particular the divertor plasma detachment control via the evolution of the enhanced high Balmer line intensities and Stark broadening high-resolution spectroscopy measurements represent a promising D&C system to preserve the divertor target integrity of the high heat flux densities effects (sputtering and deposition) [2].

In view of the unprecedented high levels of neutron and gamma fluxes, and fluences expected, together with high energy charge-exchange (c-x) atoms penetrating into diagnostic ports in DEMO [8], the location of any optical component considering the geometrical constrains at close proximity to the plasma will have a strong impact in terms of durability and imaging quality, determining its applicability for DEMO control. The focus of this paper is on the preliminary optical design of a high-resolution visible (VIS) spectrometer system for divertor plasma detachment detection via measurements of Balmer strong intensity emission lines and Stark broadening from hydrogen isotopes.

The paper is organized as follows. A brief description of the DEMO baseline model is given and the main geometrical constraints are discussed, in connection with some criteria adopted for mirror protection; relevant to the design and implementation of an optical system for imaging of

divertor plasma. As a result of this initial step, a common parametric optical layout for three optical subsystems is described as function of the image target region and wavelength range of interest, used later as input data for ZEMAX simulations. Subsequently, optics simulations results of these optical subsystems are reported and discussed. Lastly, these results are exported to a CATIA model and integrated into a simplified ITER-like diagnostic shield module (DSM) to assess its feasibility and compatibility with other diagnostics systems located at the same equatorial port (EP).

2   Divertor parallel imaging and geometrical constraints

DEMO divertor region is an area where a strong plasma-wall interaction and high fluxes of impurity particles are expected; in consequence, to ensure the protection and long-term durability of any diagnostic component responsible for the monitoring and control of plasma detachment, its location must be protected, positioned far from the divertor region. In the first instance DEMO offers two host ports possibilities for first mirror location (M), at the vertical (VP) and equatorial port (EP); however, considering that the plasma recombination in a fully detached plasma occurs at the strike point and its position could be forced by the control of the vertical plasma position, a parallel observation in poloidal orientation close to the divertor targets would allow to monitor the recombination rate through the photon emission along the main separatrix (*recombination volume*) with high imaging resolution [2]; nevertheless an oblique observation parallel to the divertor targets seems to be also suitable, providing an advantage to the observation from the EP to detect the recombination radiation, including the strike point in the field of view. Excluding the use of the VP as first option due to the geometrical limitations; instead, the implementation of this measurement is technically possible by integrating three optical subsystems into an EP, imaging the outer, x-point and inner divertor regions under oblique angles separately [9].

Whereas the plasma discharge evolution on DEMO and the physics models for future advanced control schemes are matters which will be investigated in a later design stage, in this phase a flexible approach has been adopted for a complete plasma divertor observation by means of three optical systems. In spite of that, in future, a more detailed divertor plasma shape description could suggest a reduced region of observation, leading to a reduction of the field of view and first mirror size as well.

Each of the three subsystems are devoted to transmit light in the near-UV with high spatial resolution (Δl = 3 mm) for the reconstruction of high-n Balmer lines, in particular transitions ($D_{10-2}, D_{11-2}, D_{12-2}, D_{13-2}$) for divertor detachment control and the VIS spectrum overview for plasma impurity monitoring, splitting the light in two wavelength ranges of interest and measured by two spectrometers [2].

The DEMO EP volume is configured with a width of 1,6 m and a height of 2,8 m in toroidal and poloidal direction respectively, with an interspace average length of 6,3 m. This volume has been subject of LoS analysis for parallel divertor imaging, allowing the identification of three feasible toroidal first mirror locations (OP = OPx, OPy, OPz), see table 1; separated from each other at a distance of ΔZ = 450 mm, with reference to the Z axis. A mechanical support structure has been conceptualized from an ITER-like diagnostic module with LoS completely contained within EP volume to prevent interferences with the vacuum vessel (VV) and other structures.

Table 1. First mirror locations at EP (M1, M2, M3) and target region; high field side (HFS), X-Point (XP) and low field side (LFS).

OP	OPx [mm]	OPy [mm]	OPz [mm]
M1/LFS	13500	−500	1100
M2/XP	13500	−500	650
M3/HFS	13500	−500	200

To ensure the protection of the optical components, a pinhole configuration has been adopted, with a duct opening of $\rho = 30$ mm of diameter at the Breeding Blanket (BB) and the inclusion of a Deuterium (D_2) flow of density $n_G = 3e19 m^{-3}$, whose visible absorption is negligible, through a labyrinth path (duct) for neutron shielding and erosion rate attenuation induced by high energy atoms (hydrogen fluxes) in optical components. In particular, first mirrors have been located at a distance of $L > 1240$ mm; to guarantee a large $(L/\rho) > 50$ ratio and an erosion rate of $h_{sp} < 8$ nm/fpy [10]; in addition, the use of ducts with baffles as passive methods of protection can reduce the flux of impurities on first mirrors [11], and contribute with the intensity attenuation of the light scattered by metal wall and inner duct surfaces, originating from other plasma regions.

2.1 Meridional and sagittal plane definition

The first step in designing is based in paraxial rays propagation, which are traced according to a linear approximation to Snell's Law (aberrations are neglected at this stage), considering focus effects in the meridional and sagittal planes separately; this approach describes how the two principal curvatures at every point of an optical surface are approximated by two principal curvatures at the mirror center (Coddington's equations). Therefore, sagittal and meridional plane definition is conceptualized within the constraints imposed by the EP and the plasma region under observation being fundamental for optical performance analysis.

Meridional plane has been defined by the collinearity condition of 3 points belonging to the LoS and the sagittal (orthogonal) plane has been defined as consequence of it. In practice, considering the divertor middle plane in poloidal orientation (plane X, Y = 0, Z), see figure 1 and figure 2,
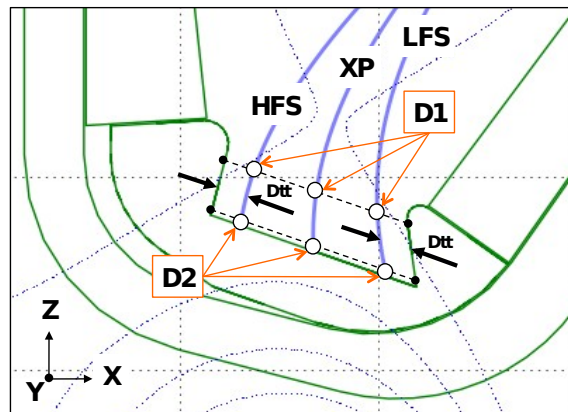

Figure 1. Divertor LoS points coordinates (D1, D2) for parallel observation (plane X, Y = 0, Z) and LoS centroids as function of the toroidal angle (φ).

Table 2. Divertor LoS points coordinates (D1, D2) for parallel observation; coordinate values are in [mm]; X and Z coordinates are extracted from figure 1, and Y* coordinates have been estimated as function of (φ) and OP coordinates reported in table 1.

	HFS (φ = 54.73°)			XP (φ = 57.11°)			LFS (φ = 60.4°)		
	X	Y*	Z	X	Y*	Z	X	Y*	Z
D1	6808	4837	−5849	7385	5554	−6082	7962	6354	−6315
D2	6642	5423	−6513	7348	6170	−6767	8053	7006	−7020

LoS centroids are constituted by a set of coordinates points (D1 = X1, Y1, Z1), (D2 = X2, Y2, Z2) located at the divertor target region and (OP = OPx, OPy, OPz) located at the EP for field mirrors locations. Points D1 and D2 are chosen parallel to the target region with a distance (Dtt = 300 mm), at the high field side (HFS) and low field side (LFS), while x-point (XP) LoS intersect the divertor center; the coordinates are reported in table 2. Consequently, OP points are located as far as possible from the plasma, within the EP according to the divertor region to be covered, see figure 2.

Bearing in mind the collinearity between vectors $\overrightarrow{OP - D1}$ and $\overrightarrow{D1 - D2}$; under the same direction as function of the toroidal angle (φ), eq. (2.1) confirm this property for the condition $f(\varphi) = 0$, with φ in the domain ($0 < \varphi \leq \pi/2$). In this way, the value of φ estimated is used to verify the suitability of OP coordinates; at this stage LoS centroids are full defined, nevertheless their paths intersect the inner first wall surface; such intersections are associated to the coordinates for duct openings at the BB, and these have been estimated numerically and graphically in figure 2, to prevent any interference with an external structure (outside of the EP). After the validation of D1, D2, and OP coordinates an arbitrary out-vessel and coplanar coordinate point has been used (SOC = SOCx, SOCy, SOCz) to define the extension of meridional and sagittal planes of solution for the observation of the HFS, XP and LFS.

$$f(\varphi) = A + B * \cos(\varphi) + C * \sin(\varphi) \tag{2.1}$$

Where:

$$S = \frac{(Z2 - OPz)}{(Z1 - OPz)}$$
$$A = \left(OPx^2 + OPy^2\right) * (1 - S)^2 + S^2 * X_1{}^2 - X_2{}^2$$
$$B = 2 * S * OPx * X_1 * (1 - S)$$
$$C = 2 * S * OPy * Y_1 * (1 - S)$$

Once the meridional and sagittal planes are defined, the optical system can be outlined and assessed through simulations oriented to optimize the image quality and resolution, but keeping in mind the tilt angle β between the DEMO Z axis and the meridional plane, required to ensure the efficient use of the EP volume in poloidal orientation.

3   Optical layout

Based on previous results, a standard and flexible optical design has been elaborated for further improvements and analysis, see figure 3; as an initial approach first optical components are represented
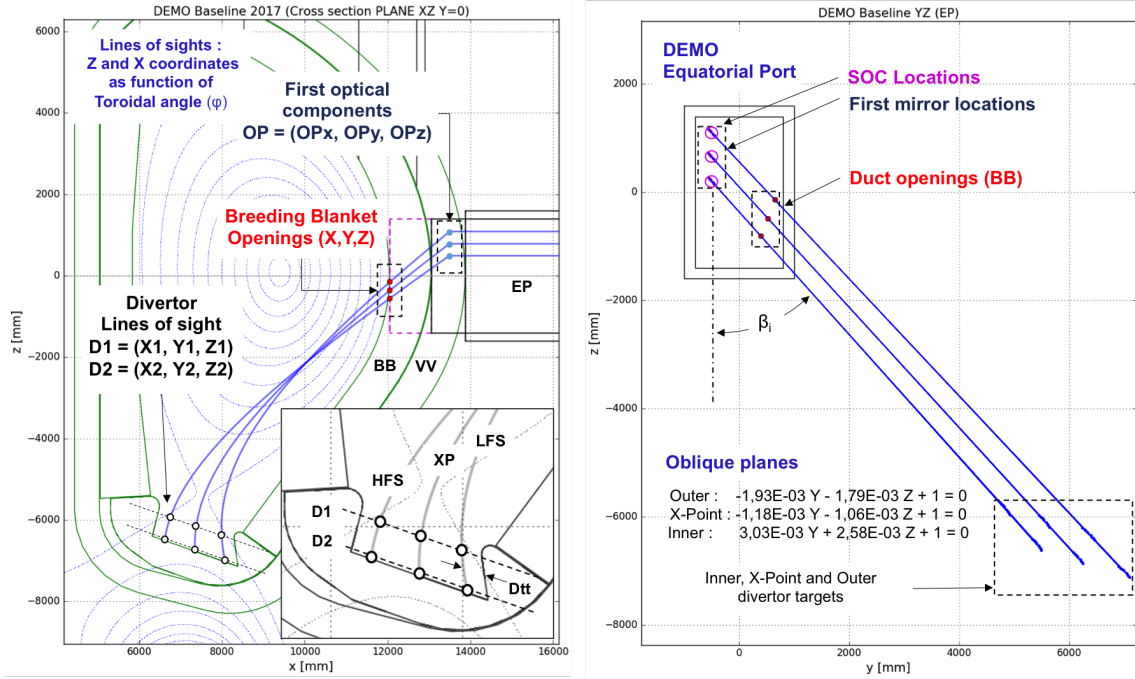
Figure 2. Divertor observation and geometrical constrains for meridional and sagittal planes.

by toroidal mirrors (M) with symmetrical meridional and sagittal focus $f_m = f_s$ and $f_{m'} = f_{s'}$; in the meridional and sagittal planes the toroidal mirror (M) focuses light rays from the divertor plasma at the mirror (A), according to the system of equations eq. (3.1); known as Coddington's equations, where fm and fm' are the object-to-toroidal mirror and the toroidal mirror-to-mirror (A) distance, respectively. R is the major radius of curvature, r the minor radius of curvature of the toroidal mirrors and α the incident angle to the mirror in the meridional plane.

$$\frac{1}{f_m} + \frac{1}{f_{m'}} = \frac{2}{R * \cos \alpha}$$
$$\frac{1}{f_s} + \frac{1}{f_{s'}} = \frac{2 * \cos \alpha}{r}$$

(3.1)

Secondary optical components location are distributed along a labyrinth path within ducts with miter bend connections [12]; for a multi-configuration optical simulation, the initial conditions for some values such as radius of curvatures, optical focuses, component distances and expected integrated solid angle (Ω) subtended by the mirror (M) with respect to a isotropic radiating linear source (O) are summarized in table 3 and table 4. The entire system consists of three optical subsystems for HFS, XP and LFS divertor parallel, whose depths of field (DOF) are 353 mm, 384 mm and 292 mm respectively.

The initial approach laid down in this design was the light propagation through the reflection of four planar mirrors (A, B, C, D), from (M) to (S1-Port plug), to avoid the introduction of aberrations. As a result of this test, the image resolution obtained at (S2) was near to 3 mm with a beam radius of around 400 mm. Subsequently in order to reduce the beam radius and get a more compact
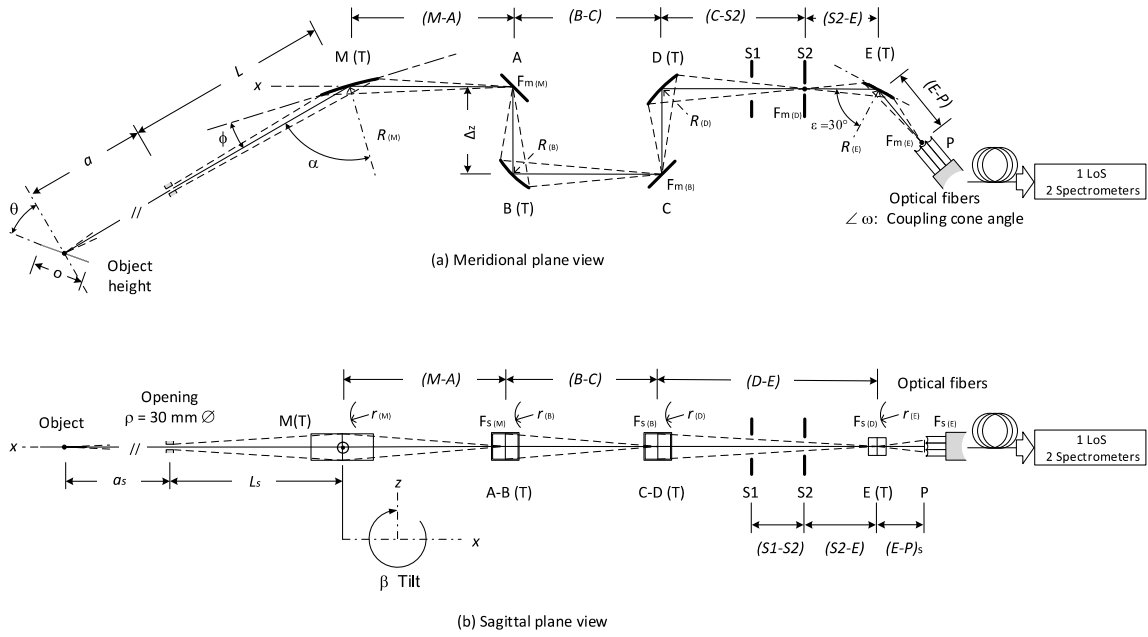
Figure 3. Common optical layout for high-resolution divertor spectroscopy, (a) Meridional plane of view and (b) sagittal plane view.

Table 3. Optical layout (dimension properties).

Configure	S [mm]	L [mm]	M-A [mm]	ΔZ [mm]	B-C [mm]	C-S2 [mm]	S1-S2, S2-E, E-P [mm]	O [mm]	θ [Deg]	α [Deg]	β [Deg]	Ω [mSr]
Outer	12366	2232	1400		2200	1250		802	26,19	65,38	42,75	3,6
X-point	11634	2148	950	450	3100	800	500	790	28,71	66,82	41,97	4,1
Inner	11071	2103	500		4000	350		763	21,41	68,59	41,42	4,6

optical setup, toroidal mirrors have been included at B, D and E locations for intermediate imaging. Theoretical values are summarized in table 4.

The implementation of optical fibers at the location (P), see figure 3, is subordinated to the irradiation levels and *displacements per atoms* (dpa) induced by neutrons on glass expected in this region and also the effects on the optical properties of materials to be used as transmission components [13]. Alternatively, metallic mirrors could be included, separated by a diamond window or within vacuum extensions to transport the light at safe places for optical fibers [14]. In addition to the use of diamond as hydrogen isotope barrier, diamond windows exhibits an extraordinary thermal conductivity and its transmission starts in the UV at 225 nm, covering the entire spectral range, from the visible through the infrared and terahertz range up to radar frequencies.

3.1 ZEMAX simulations

A set of multi-configuration simulations have been done, using the optic layout developed in the previous section, see figure 3. Table 5 summarizes the field of observation coordinates simplified to represent the object height (plasma region) with a length (O) for each optical configuration, see

Table 4. Optical layout (Focuses and radii of curvature).

Mirror	Target	Fm=Fs [mm]	Fs' [mm]	Fm' [mm]	φ [Deg]	R [mm]	r [mm]
M	Outer	14598	1400	1400	24,62	6132	1065
	X-point	13782	950	950	23,18	4515	700
	Inner	13174	500	500	21,41	2640	352
B	Outer	450	2200	2200		1057	529
	X-point	450	3100	3100	45	1111	556
	Inner	450	4000	4000		1144	572
D	Outer	450	2250	1750		1012	530
	X-point	450	1800	1300	45	946	509
	Inner	450	1350	850		832	477
E	Outer	500	500	500		1000	250
	X-point	500	500	500	60	1000	250
	Inner	500	500	500		1000	250

Table 5. Field of observation (Object: Divertor parallel target discretized in 9 points with field 5* as centroid).

Fields	(X,Y) [mm]
1	(0,−400)
2	(0,−300)
3	(0,−200)
4	(0,−100)
5*	(0,0)
6	(0,100)
7	(0,200)
8	(0,300)
9	(0,400)

table 3. The entrance pupil aperture (Stop) has been set to 30 mm of diameter and parallel-oriented to DEMO Z axis, with uniform illumination in VIS wavelength range within an environment at 20°C and 1 atm.

Field 5 represents the centroid of the system, and reference for optimization and parallelism between the subsystems at the interspace. An initial tilted surface has been used to define the object (O) and its fields of observation; this plane is defined in terms of the tangent angle (θ) between the normal plane to the centroid and the object, as well as the projection of it on the divertor. Toroidal surfaces have been used at locations (M, B, D, E) to reduce the beam dimensions by defining the curvature in the meridional (R) and sagittal (r) planes, eq. (3.1); spherical optical surfaces with infinite radius of curvature (ZEMAX standard surface) have been used for planes mirrors at locations (A, C) to ensure a free light propagation, and coordinate breaks surfaces to compensate changes of beam direction. ZEMAX 3D layout in figure 4 and figure 5, shows the integration of all
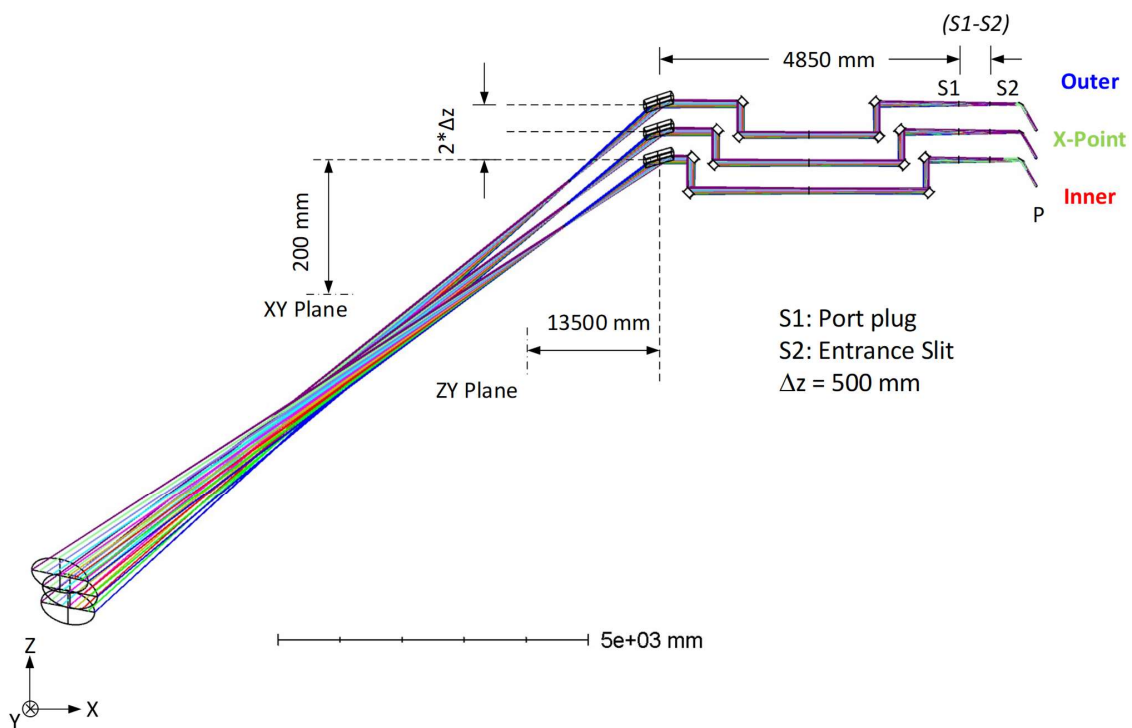
Figure 4. DEMO High-resolution system for plasma divertor parallel observation ZEMAX 3D layout, ZX plane.
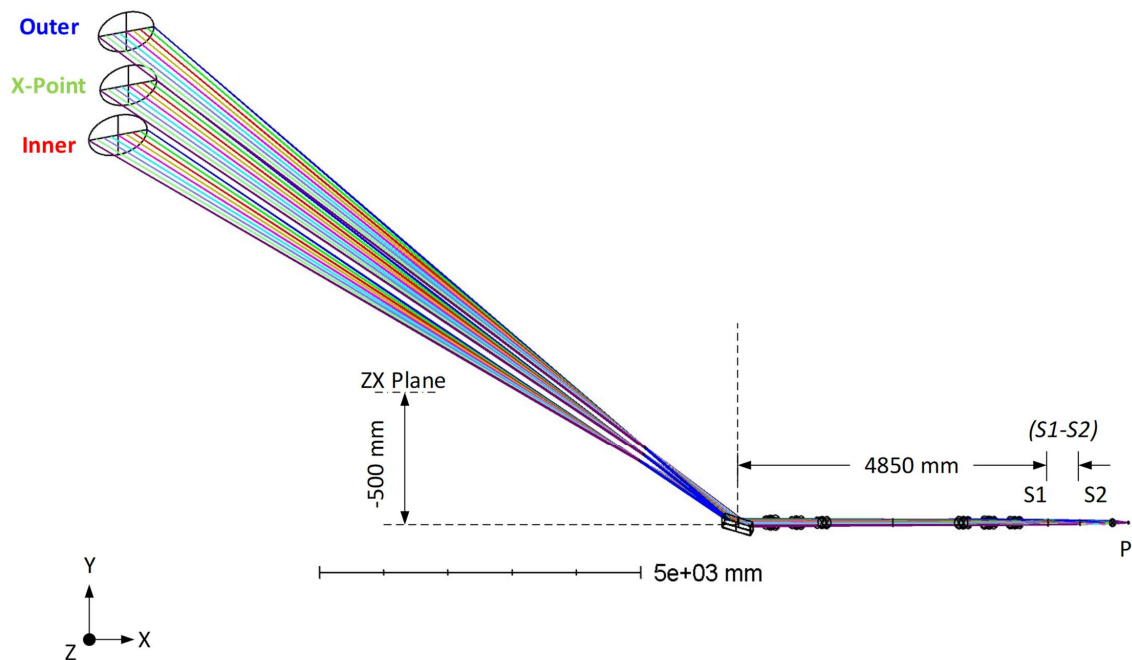
Figure 5. DEMO High-resolution system for plasma divertor parallel observation ZEMAX 3D layout, YX plane.

Table 6. Results (Mirror dimensions by subsystem).

Target: outer divertor						
Mirror	M	A	B	C	D	E
Diameter [mm]	223	90	85	91	95	44
Z [mm]	164	66	63	67	70	33
Y [mm]	152	61	58	62	65	30
Target: X-Point						
Mirror	M	A	B	C	D	E
Diameter [mm]	241	100	90	96	100	55
Z [mm]	179	75	67	71	74	41
Y [mm]	161	67	60	64	69	37
Target: inner divertor						
Mirror	M	A	B	C	D	E
Diameter [mm]	267	113	99	92	95	65
Z [mm]	200	84	74	69	71	49
Y [mm]	177	74	65	61	63	43

subsystems in the planes ZX and YX; with an offset between them of X=0; Y= ΔZ, and Z=0; LoS colors represent fields of observation, from surface defined as *Object* to surface *Image* at point (P).

Single crystal (SC) molybdenum (Mo) and rhodium (Rh) mirrors are considered as the most promising resources for first mirror material due to their good thermal properties, low sputtering yield and good reflectivity in the visible wavelength range [15, 16]; these materials have been defined in ZEMAX and modeled as coating, considering that any interaction with light occurs primarily within a few nanometers of the surface. The following table 6, shows the mirror dimensions by subsystem, as a result of the root mean square (RMS) spot radius optimization; considering the tilt angle β, see table 2; the projected length in Z and Y axis are estimated; projected values on Y axis will determine the over-all shape and size of the DSM.

The scope of this section concludes with the imaging at the location (P), see figure 6. Where the footprint diagram displays the beam result of every subsystem superimposed on surface *Image*. This image has been resolved with a Δl = Object height/# fields of observation $\approx$ 90 mm, exhibiting a loss of resolution compared to the first approach, in which assuming only plane mirrors a spatial resolution of Δl = 3 mm appears achievable. Mirror radii have been optimized from the initial values given in table 3; decimals have been rounded to the next integer, assuming a curvature tolerance between 0,8% and 1%, at this phase of design, achieving a demagnification factor around 800 : 36 $\approx$ 20. Rays aberrations and spot analysis offer a wide variety of powerful tools to improve the performance of the system, in terms of resolution and space occupation, issues that will be assessed in subsequent steps of this preliminary design.

From figure 6, we can observe changes of size and shape between the spot images at distances represented by the nearest and the farthest fields of observation due to its DOFs and the RMS-radius value shows in the spot diagram; considering that the centroid of each system has been used as subject of optimization, the spot sizes and shapes at the ends (top and botton) are a realistic measure
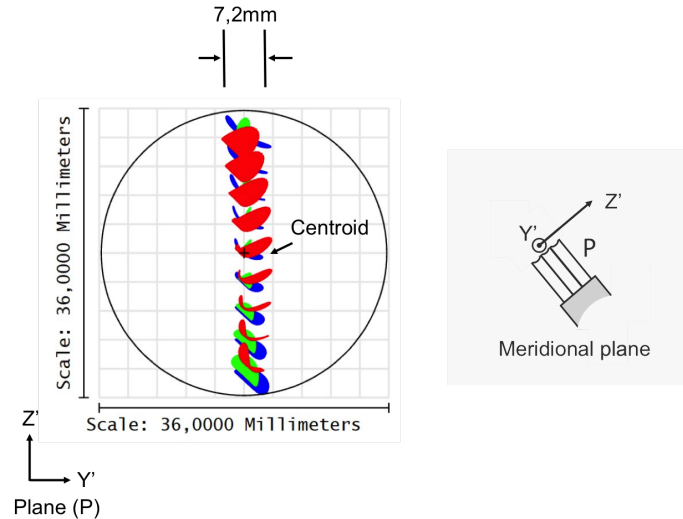
Figure 6. Imaging and footprint spot diagram overview at location (P).

of the resolution to be expected including all aberrations; for instance in the case of the inner spot diagram (red), top-end spots are in contact, revealing the limit of spatial resolution for this optical configuration. The imaging at the location (P) represents the starting point for the next phases of design in which a more realistic plasma scenario and physical constrains should be define in the light of a non-linear process of design, heavily dependent on critical parameters such as: temporal response and precision [17].

4 ITER-like diagnostic module

In the previous section, the optical performance is described by the optimization of a ZEMAX RMS spot radius merit function, with a strong dependence on variables that are not yet defined, such as: operation temperature, mechanical tolerances, mirror material and reflectivity; without mentioning the high sensibility to the initial values assumed during the optimization process, and the aberrations introduced by the use of curved mirrors and tilt angles. Nevertheless, the numerical assessment of these offer a preliminary idea about the main challenges posed by the conceptual design in terms of feasibility, space required by mirrors, light beam dimensions, shielding scheme and the identification of thermal critical zones.

The change of the optical reflectivity of mirror surfaces due to the operation temperature for this case could be omitted; considering that this effect is evidenced for temperatures higher than three-quarters of the melting point, and whose values for Rh and Mo are around 1473°C and 1967°C respectively; temperatures values that can be controlled via a dedicated water cooling circuit, given an induced power density $\leq 1\,[\text{W/cm}^3]$ at radial distances from the first wall (FW) to the mirror locations greater than 1 meter, behind long ducts and surrounded by shielding material. The above statement has been derived from the neutronic analysis and the interpolation of the nuclear power density induced by neutrons on steel at the back of the BB modules on DEMO [18], where a power density attenuation from 9 to $1\,[\text{W/cm}^3]$ is expected; however, it is important to note that neutronic
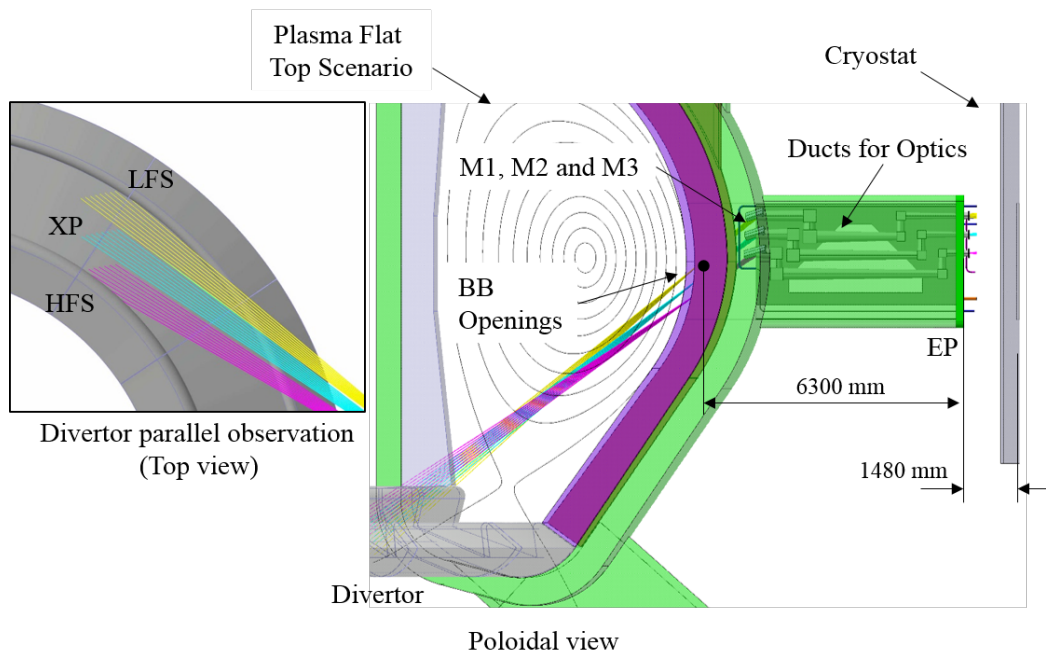
Figure 7. Divertor parallel observation and DSM integration on DEMO baseline 2017.

transport at the EP is determined by the structural configuration, therefore, an accurate power density factor can only be estimated by means of a more detailed radiation transport simulation model.

A simplified ITER-like diagnostic module has been conceptualized, based on three parameterized labyrinth paths for optics; within a central shield block protected by three ducts with miter bend connections [7] and a lateral common (Cu) cool plate (Thermal sink) to ensure the control on the operation temperature of the mirrors. figure 7 shows an overview integration of it on DEMO baseline 2017 model in flat-top plasma scenario [5]; main distances and LoS for divertor parallel observation are indicated as well.

The diagnostic module integration at EP shows a limited space to host more than two D&C systems with similar dimensions (about 760 mm in width). The idea of a full-dedicated EP for divertor plasma control includes the application of a thermography system (outer and inner divertor target) in poloidal orientation, additionally; a core spectroscopy system is foreseen to share the same EP volume with their respective calibration systems. This rough draft is envisaged to be initial designs, aimed at introducing the main R&D critical aspects under a system engineering approach, see figure 8.

According to the mirror locations, three areas have been identified as critical for temperature control, where the heat induced by neutrons must be removed effectively to ensure the minimum thermal expansion on mirrors. To this end, two separates cooling circuits have been proposed, the first to provide cooling at the first mirror locations (M1, M2, M3 — Z1), and the second one, to provide cooling at the locations (A, B — Z2) and (C, D — Z3) in parallel. Drops in pressure, mass flow rate and other details are issues which need to be investigated in an advanced stage of design. In addition, an inlet pipe of D_2 gas has been included as an out-vessel connection to supply all the system in parallel, simplifying any possible intervention by remote handling.
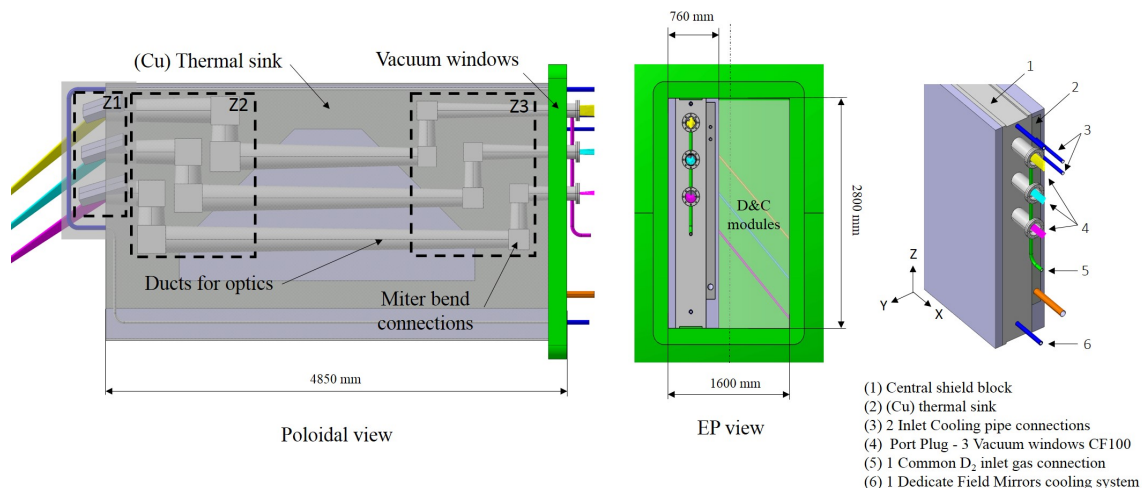
Figure 8. ITER-like module: poloidal and equatorial port views, space occupation and DSM description.

5 Conclusions

Exhaust plasma divertor control represents one of the most important challenges for DEMO D&C. The implementation of a robust high-resolution spectroscopic system for parallel divertor plasma observation has been introduced and a preliminary optical design concept based on plane and toroidal mirrors proposed, aimed to measure the plasma radiation emission in the NUV/VIS range, following the evolution of the enhanced high Balmer line intensities and Stark broadening as indicators of high density plasma (plasma detachment) [1, 2]. The system presented for the observation of the whole divertor region is a combination of three parallel imaging optical systems with demagnification factor around ≈ 20 in poloidal orientation, protected from neutrons within labyrinth/shielded paths (ducts) with a gas target density $n_{\rm G} = 3e19 m^{-3}$ [8]. The location of the mirrors has been parameterized to simplify and optimize the space required. Consequently, imaging simulations have been developed in two steps, initially focusing on the free ray light propagation using planar mirrors and secondly with the intention to reduce the beam dimensions, by the inclusion of toroidal mirrors for an intermediate imaging. Relevant optical dimensions are reported and an ITER-like diagnostic module is proposed.

Acknowledgments

References

[1] W. Biel, R. Albanese, R. Ambrosino, M. Ariola, M. Berkel, I. Bolshakova et al., *Diagnostics for plasma control – from ITER to DEMO*, Fusion Eng. Des. **146** (2019) 465.

[2] A. Meigs, S. Brezinsek, M. Clever, A. Huber, S. Marsen, C. Nicholas et al., *Deuterium balmer/stark spectroscopy and impurity profiles: First results from mirror-link divertor spectroscopy system on the JET ITER-like wall*, *J. Nucl. Mat.* **438** (2013) S607.

[3] B.L. Welch, H.R. Griem, J. Terry, C. Kurz, B. LaBombard, B. Lipschultz et al., *Density measurements in the edge, divertor and X-point regions of Alcator C-Mod from Balmer series emission*, *Phys. Plasmas* **2** (1995) 4246.

[4] S. Salasca, M.-H. Aumeunier, F. Benoit, B. Cantone, Y. Corre, E. Delchambre et al., *The ITER equatorial visible/infra-red wide angle viewing system: Status of design and R&D*, *Fusion Eng. Des.* **96-97** (2015) 932.

[5] G. Federici, R. Kemp, D. Ward, C. Bachmann, T. Franke, S. Gonzalez et al., *Overview of EU DEMO design and r&d activities*, *Fusion Eng. Des.* **89** (2014) 882.

[6] W. Biel, M. de Baar, A. Dinklage, F. Felici, R. König, H. Meister et al., *DEMO diagnostics and burn control*, *Fusion Eng. Des.* **96-97** (2015) 8.

[7] A. Donné, A. Costley and A. Morris, *Diagnostics for plasma control on DEMO: challenges of implementation*, *Nucl. Fusion* **52** (2012) 074015.

[8] M. Tokar, *Assessment for erosion of and impurity deposition on first mirrors in a fusion reactor*, *Nucl. Fusion* **58** (2018) 096007.

[9] G. Matthews, *Plasma detachment from divertor targets and limiters*, *J. Nucl. Mat.* **220-222** (1995) 104.

[10] W. Gonzalez, W. Biel, P. Mertens, M. Tokar, O. Marchuk and C. Linsmeier, *Conceptual studies on spectroscopy and radiation diagnostic systems for plasma control on DEMO*, *Fusion Eng. Des.* **146** (2019) 2297.

[11] V. Kotov, D. Reiter, A. Litnovsky, A. Krimmer, A. Kirschner and Y. Krasikov, *Passive protection of the ITER diagnostic mirrors*, *Phys. Scr.* **T145** (2011) 014071.

[12] A. Lopes, R. Luís, E. Klinkby, E. Nonbøl, M. Jessen, R. Moutinho et al., *Neutronics analysis of the ITER collective thomson scattering system*, *Fusion Eng. Des.* **134** (2018) 22.

[13] G. Vayakis, E.R. Hodgson, V. Voitsenya and C. I. Walker, *Chapter 12: Generic diagnostic issues for a burning plasma experiment*, *Fusion Sci. Technol.* **53** (2008) 699.

[14] K. Ujihara, *Reflectivity of metals at high temperatures*, *J. Appl. Phys.* **43** (1972) 2376.

[15] J. Peng, A. Litnovsky, A. Kreter, Y. Krasikov, M. Rasinski, U. Breuer et al., *Sputtering tests of single crystal molybdenum and rhodium mirrors at high ion fluence for in situ plasma cleaning of first mirrors in ITER*, *Fusion Eng. Des.* **128** (2018) 107.

[16] L. Marot, G.D. Temmerman, P. Oelhafen, G. Covarel and A. Litnovsky, *Rhodium coated mirrors deposited by magnetron sputtering for fusion applications*, *Rev. Sci. Instrum.* **78** (2007) 103507.

[17] A. Scheeline, *How to design a spectrometer*, *Appl. Spectrosc.* **71** (2017) 2237.

[18] U. Fischer, C. Bachmann, J.-C. Jaboulay, F. Moro, I. Palermo, P. Pereslavtsev et al., *Neutronic performance issues of the breeding blanket options for the european DEMO fusion power plant*, *Fusion Eng. Des.* **109-111** (2016) 1458.